Direct Voltage Control of DC-DC Boost Converters Using Enumeration-Based Model Predictive Control

Petros Karamanakos, *Student Member, IEEE*, Tobias Geyer, *Senior Member, IEEE*, and Stefanos Manias, *Fellow, IEEE*

***Abstract*—This paper presents a model predictive control (MPC) approach for dc-dc boost converters. A discrete-time switched non-linear (hybrid) model of the converter is derived, which captures both the continuous and the discontinuous conduction mode. The controller synthesis is achieved by formulating an objective function that is to be minimized subject to the model dynamics. The proposed MPC strategy, utilized as a voltage-mode controller, achieves regulation of the output voltage to its reference, without requiring a subsequent current control loop. Furthermore, a state estimation scheme is implemented that addresses load uncertainties and model mismatches. Simulation and experimental results are provided to demonstrate the merits of the proposed control methodology, which include a fast transient response and a high degree of robustness.**

***Index Terms*—DC-DC boost converter, model predictive control (MPC), optimal control, voltage control, hybrid system.**

I. Introduction

OVER the past decades dc-dc conversion has matured into a ubiquitous technology, which is used in a wide variety of applications, including dc power supplies and dc motor drives [1]. Dc-dc converters are intrinsically difficult to control due to their switching behavior, constituting a (continuous-time) switched linear or *hybrid* system. To date, a plethora of control schemes has been proposed to address these difficulties. These control techniques range from linear techniques, such as proportional-integral (PI) controllers based on average models [2], [3] to fuzzy logic [4], [5], and from non-linear techniques [6], [7] and feedforward control [8], [9] to sliding mode [10], [11] and H_∞ methods [12].

Although existing control approaches have been shown to be reasonably effective, several challenges have not been fully addressed yet, such as ease of controller design and tuning, as well as robustness to load parameter variations. Furthermore, the computational power available today and the recent theoretical advances with regards to controlling hybrid systems allow one to tackle these problems in a novel way. The aim is not only to improve the performance of the closed-loop system, but to also enable a systematic design and implementation procedure. Model predictive control (MPC) is a particularly promising candidate to achieve this [13], [14], since it allows one to directly include constraints in the design phase and to address the switching or hybrid nature of dc-dc converters. MPC was developed in the 1970s in the process control industry, and has recently been introduced to the field of power electronics, including three-phase dc-ac and ac-dc systems [15]–[20], as well as dc-dc converters [21]–[30].

In MPC the control action is obtained by solving online at each time-step an optimization problem with a given objective function over a finite prediction horizon, subject to the discrete-time model of the system and constraints. The optimal sequence of control inputs is the one that minimizes the objective function. To provide feedback, allowing one to cope with model uncertainties and disturbances, only the first element of the sequence of control inputs is applied to the converter. At the next time-step, the optimization problem is repeated with updated measurements or estimates. This procedure is known as the *receding horizon policy* [14].

In this paper, MPC is employed as a voltage-mode controller for the dc-dc boost converter. The main control objective is the regulation of the output voltage to a commanded value, while rejecting the impact of variations in the input voltage and the load. The discrete-time model of the converter used by the controller is designed such that it accurately predicts the plant behavior both when operating in continuous (CCM) as well as in discontinuous conduction mode (DCM). As a result, the formulated controller is applicable to the whole operating regime, rather than just to a particular operating point. To address time-varying and unknown loads, a Kalman filter is added that estimates the converter states and provides offset-free tracking of the output voltage due to its integrating action, despite changes in the load [31]. In that way the robustness of the controller is ensured even when the converter operates under non-nominal conditions.

The proposed scheme carries several benefits. The very fast dynamics achieved by MPC, combined with its inherent robustness properties, are some of its key beneficial characteristics. Furthermore, thanks to the fact that the control objectives are expressed in the objective function in a straightforward manner, the design process is simple and laborious tuning is avoided. The inherent computational complexity is the most prominent drawback—the computational power required increases exponentially as the prediction horizon is extended. To address this issue, a move blocking strategy is adopted [32], which results in a significant reduction of the computations required and facilitates the real-time implementation of the controller. Finally, the absence of a modulator and the direct manipulation of the converter switches imply a variable switching frequency.

P. Karamanakos and S. Manias are with the Department of Electrical and Computer Engineering, National Technical University of Athens, 15780 Zografou, Athens, Greece (e-mail: petkar@central.ntua.gr; manias@central.ntua.gr).

T. Geyer is with ABB Corporate Research, 5405 Baden-Dättwil, Switzerland (e-mail: t.geyer@ieee.org).

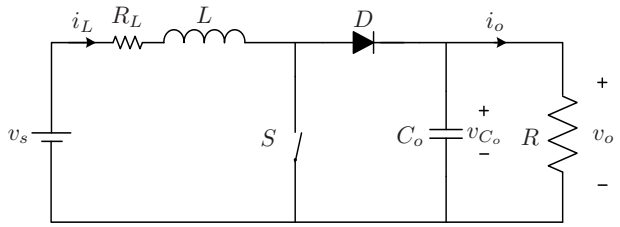

Fig. 1. Topology of the dc-dc boost converter.

This paper is organized as follows. In Section II the continuous-time model of the converter, suitable for both CCM and DCM, is presented. Furthermore, the discrete-time model that will be used as the prediction model is derived. The control problem is stated in Section III. In Section IV, the MPC problem is formulated and solved, using a move blocking scheme and enumeration, and a Kalman filter is added to address load variations. Section V presents simulation results illustrating the performance of the proposed control approach. In Section VI, the experimental validation of the introduced control strategy is provided. The paper is summarized in Section VII, where conclusions are drawn.

II. Model of the Boost Converter

A. Continuous-Time Model

The dc-dc boost converter shown in Fig. 1 is a converter that increases the (typically uncontrolled) dc input voltage $v_s(t)$ to a higher (controlled) dc output voltage $v_o(t)$. The converter consists of two power semiconductors—the controllable switch S, and the diode D. The inductor L with the internal resistor R_L is used to store and deliver energy depending on the operating mode of the converter, while the filter capacitor C_o is connected in parallel with the load resistor R so as to ensure a constant output voltage during steady-state operation of the converter.

Three different linear dynamics are associated with the switch positions. When the switch S is *on* ($S = 1$), energy is stored in the inductor L and the inductor current $i_L(t)$ increases. When the switch S is *off* ($S = 0$), the inductor is connected to the output and energy is released through it to the load, resulting in a decreasing $i_L(t)$. Furthermore, when the switch S remains *off* and $i_L(t) = 0$, then both S and D are *off*; the topology is reduced to the mesh formed by the capacitor C_o and the load. In this case, the converter operates in DCM.

The state-space representation of the converter in the continuous-time domain is given by the following equations [33]

$$\frac{dx(t)}{dt} = \big(A_1 + A_2 u(t)\big)x(t) + Bv_s(t) \tag{1a}$$

$$y(t) = Cx(t)\,, \tag{1b}$$

where

$$x(t) = [i_L(t)\ v_o(t)]^T \tag{2}$$

is the state vector, encompassing the inductor current and the output voltage across the output capacitor. The output

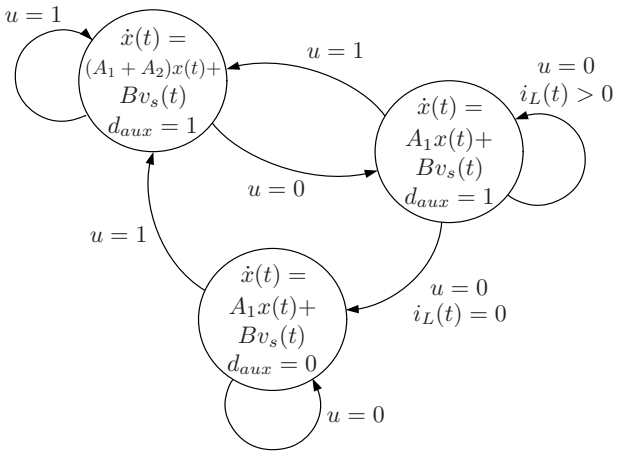

Fig. 2. Dc-dc converter presented as a continuous-time automaton.

$y = v_o(t)$ is given by the output voltage. The system matrices are

$$A_1 = \begin{bmatrix} -\frac{d_{aux}R_L}{L} & -\frac{d_{aux}}{L} \\ \frac{d_{aux}}{C_o} & -\frac{1}{C_oR} \end{bmatrix}, \quad A_2 = \begin{bmatrix} 0 & \frac{1}{L} \\ -\frac{1}{C_o} & 0 \end{bmatrix},$$

$$B = [\frac{d_{aux}}{L}\ 0]^T, \quad \text{and} \quad C = [0\ 1]\,.$$

The variable u denotes the switch position, with $u = 1$ implying that the switch S is *on*, and $u = 0$ referring to the case where the switch S is *off*. Finally, d_{aux} is an auxiliary binary variable [34] that is $d_{aux} = 1$ when the converter operates in CCM, i.e. either $u = 1$ or $u = 0$ and $i_L(t) > 0$. When the converter operates in DCM, i.e. $u = 0$ and $i_L(t) = 0$, then $d_{aux} = 0$ holds.

$$d_{aux}(t) = \begin{cases} 1 & \text{if } u(t) = 1, \text{ or } u(t) = 0 \text{ and } i_L(t) > 0 \\ 0 & \text{if } u(t) = 0 \text{ and } i_L(t) = 0 \end{cases} \tag{3}$$

For a graphical summary, representing the boost converter as an automaton, see Fig. 2.

B. Discrete-Time Model

The derivation of an adequate model of the boost converter to serve as an internal prediction model for MPC is of fundamental importance. As can be seen in Fig. 3, after the discretization of the model in time, the converter can operate in four different modes, depending on the shape of the inductor current. In order to precisely describe the operating modes of the converter, the matrices $\Gamma_1 = A_1$ for $d_{aux} = 1$, $\Gamma_2 = A_1$ for $d_{aux} = 0$, $\Gamma_3 = A_2$, and $\Delta = B$ for $d_{aux} = 1$ are introduced. Then, based on the continuous-time state-space model (1) and using the forward Euler approximation approach, the following discrete-time model of the converter is derived.

$$x(k+1) = \begin{cases} E_1x(k) + F_1v_s(k) & \text{Mode “1”} \\ E_2x(k) + F_2v_s(k) & \text{Mode “2”} \\ E_3x(k) + F_3v_s(k) & \text{Mode “3”} \\ E_4x(k) & \text{Mode “4”} \end{cases} \tag{4a}$$

$$y(k) = Gx(k) \tag{4b}$$

where the matrices are $E_1 = \mathbf{1} + (\Gamma_1 + \Gamma_3)T_s$, $E_2 = \mathbf{1} + \Gamma_1T_s$, $E_3 = \frac{1}{T_s}(\tau_1E_2 + \tau_2E_4)$, $E_4 = \mathbf{1} + \Gamma_2T_s$,

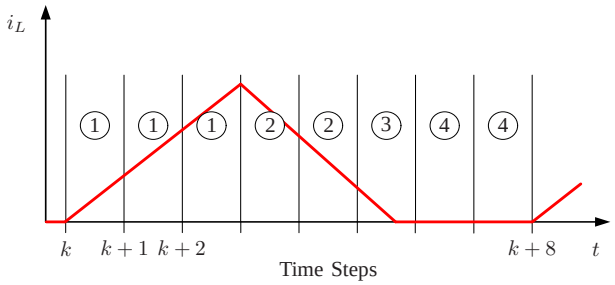

(a) Current.

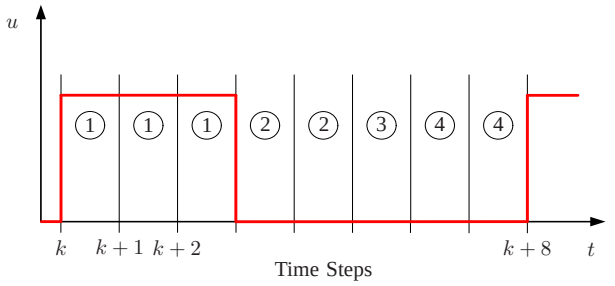

(b) Switch position.

Fig. 3. Operation modes used in the mathematical model to describe the boost converter. Depending on the shape of the current four different modes are used.

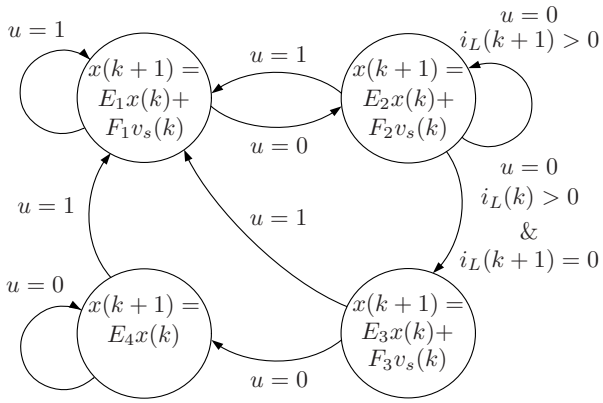

Fig. 4. Discrete-time mathematical model of the dc-dc converter represented as a discrete-time automaton.

$F_1 = \Delta T_s$, $F_2 = F_1$, $F_3 = \Delta\tau_1$, and $G = C$. Furthermore, τ_1 denotes the time-instant within the sampling interval, when the inductor current reaches zero, i.e. $i_L(k + \tau_1/T_s) = 0$, and $\tau_1 + \tau_2 = T_s$. Finally, $\mathbf{1}$ is the identity matrix and T_s is the sampling interval. Note that E_3 is derived by averaging over modes "2" and "4".

The four different operating modes of the converter's mathematical model are illustrated in Fig. 4. The transitions from one mode to another are specified by conditions, such as the switch position and the value of the current.

III. Control Problem

For the dc-dc converter, the main control objective is for the output voltage to accurately track its given reference—or equivalently to minimize the output voltage error—by appropriately manipulating the switch. This is to be achieved despite changes in the input voltage and load. During transients, the output voltage is to be regulated to its new reference value as fast and with as little overshoot as possible.

IV. Model Predictive Control

In this section an MPC scheme for dc-dc boost converters is introduced, which directly controls the output voltage by manipulating the switch S. Using an enumeration technique, the user-defined objective function is minimized subject to the converter dynamics.

A. Objective Function

The objective function is chosen as

$$J(k) = \sum_{\ell=k}^{k+N-1} \Big(|v_{o,err}(\ell+1|k)| + \lambda |\Delta u(\ell|k)| \Big) \qquad (5)$$

which penalizes the absolute values of the variables of concern over the prediction horizon N, which is of finite length. The first term penalizes the absolute value of the output voltage error

$$v_{o,err}(k) = v_{o,ref} - v_o(k)\,. \qquad (6)$$

By penalizing the difference between two consecutive switching states, the second term aims at decreasing the switching frequency and avoiding excessive switching

$$\Delta u(k) = u(k) - u(k-1)\,. \qquad (7)$$

The weighting factor $\lambda > 0$ sets the trade-off between output voltage error and switching frequency, f_{sw}. Note that the sampling interval T_s implicitly imposes an upper bound on the switching frequency, i.e. $f_{sw} < 1/(2T_s)$. This value corresponds to the case when $\lambda = 0$, the output voltage is twice the input voltage, i.e. $v_o = 2v_s$, and when the inductor is ideal with $R_L = 0$.

B. Optimization Problem

The optimization problem underlying MPC at time-step k amounts to minimizing the objective function (5) subject to the converter model dynamics

$$\begin{aligned} U^*(k) &= \arg\min J(k) \\ &\text{subject to eq. (4)}\,. \end{aligned} \qquad (8)$$

The optimization variable is the sequence of switching states over the horizon, which is $U(k) = [u(k)\ u(k+1) \ldots u(k+N-1)]^T$. Minimizing (8) yields the optimal switching sequence $U^*(k)$. Out of this sequence, the first element $u^*(k)$ is applied to the converter. The procedure is repeated at $k+1$, based on new measurements acquired at the following sampling instance.

Minimizing (8) is a challenging task, since it is a mixed-integer non-linear optimization problem[1]. A straightforward alternative is to solve (8) using enumeration, which involves the following three steps. First, by considering all possible

[1]It should be noted that the mathematical model of the converter given by (4a) for modes "1" and "2" is affine (linear plus offset), and for mode "4" is linear, while the expression for mode "3" is non-linear.

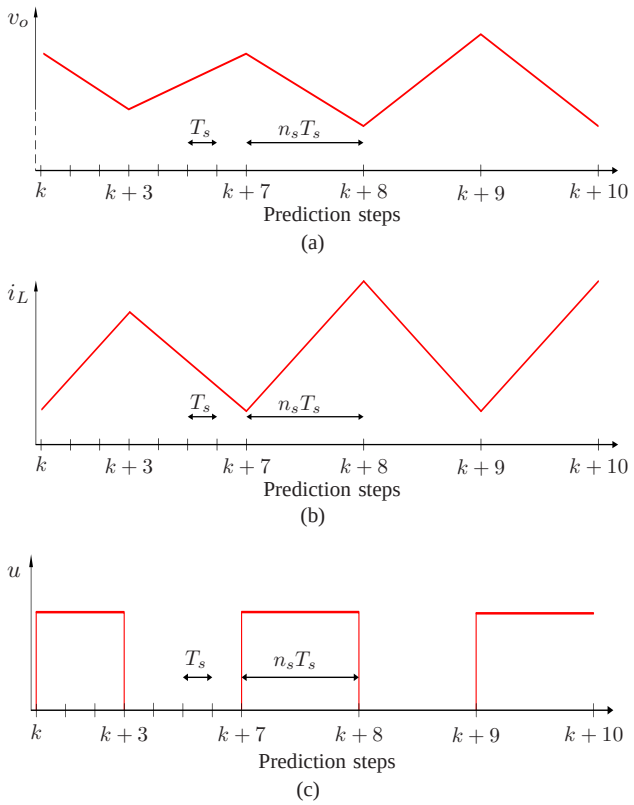

Fig. 5. Prediction horizon with move blocking: a) output voltage, b) inductor current, and c) control input. The prediction horizon has $N = 10$ time-steps, but the prediction interval is of length $19T_s$, since $n_s = 4$ is used for the last $N_2 = 3$ steps.

combinations of the switching states ($u = 0$ or $u = 1$) over the prediction horizon, the set of admissible switching sequences is assembled. For each of the 2^N sequences, the corresponding output voltage trajectory is predicted and the objective function is evaluated. The optimal switching sequence is obtained by choosing the one with the smallest associated cost.

C. Move Blocking

A fundamental difficulty associated with boost converters arises when controlling their output voltage without an intermediate current control loop, since the output voltage exhibits a non-minimum phase behavior with respect to the switching action. For example, when increasing the output voltage, the duty cycle of switch S has to be ramped up, but initially the output voltage drops before increasing. This implies that the sign of the gain (from the duty cycle to the output voltage) is not always positive.

To overcome this obstacle and to ensure closed-loop stability, a sufficiently long prediction interval NT_s is required, so that the controller can "see" beyond the initial voltage drop when contemplating to increase the duty cycle. On the one hand, increasing N leads to an exponential increase in the number of switching sequences to be considered and thus dramatically increases the number of calculations needed. On the other hand, long sampling intervals T_s reduce the resolution of the possible switching instants, since switching can only be performed at the sampling instants.

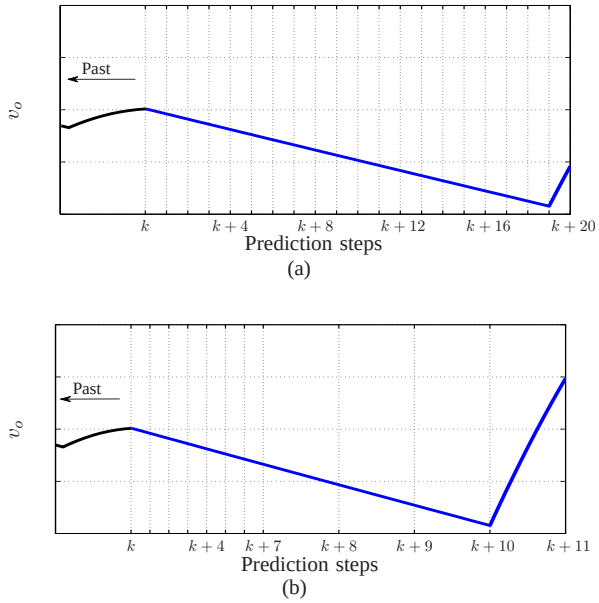

Fig. 6. Effect of the move blocking scheme. In (a), without move blocking, a prediction horizon of $N = 20$ steps of equal time-intervals is needed. In (b), with the move blocking strategy employed, an $N = 11$ prediction horizon is sufficient to achieve the same closed-loop result ($N_1 = 7$, $N_2 = 4$, and $n_s = 4$, total length $23T_s$).

A long prediction interval NT_s with a small N and a small T_s can be achieved by employing a *move blocking* technique [32]. For the first steps in the prediction horizon, the prediction model is sampled with T_s, while for steps far in the future, the model is sampled more coarsely with a multiple of T_s, i.e. n_sT_s, with $n_s \in \mathbb{N}^+$ [35]. As a result, different sampling intervals are used within the prediction horizon, as illustrated in Fig. 5. We use N_1 to denote the number of prediction steps in the first part of the horizon, which are sampled with T_s. Accordingly, N_2 refers to the number of steps in the last part of the horizon, sampled with n_sT_s. The total number of time-steps in the horizon is $N = N_1 + N_2$.

An illustrative example of the effectiveness of the move blocking strategy is depicted in Fig 6. Assume that at time instant kT_s the output voltage reference increases in a stepwise manner and the output voltage is to follow that change. However, as mentioned above, because of the non-minimum phase nature of the system, the output voltage initially tends to decrease. In order to ensure that MPC is able to predict the final voltage increase and will thus pick the corresponding switching sequence that achieves this, in this example, a prediction interval of twenty time-steps is required, i.e. $NT_s = 20$.

By employing the move blocking scheme, the eleven-step horizon $N = 11$, with $N_1 = 7$, $N_2 = 4$, and $n_s = 4$ suffices, resulting in a prediction interval of a 23 time-steps. In this way, the computational cost is significantly reduced. Without move blocking, the number of switching sequences to be examined is $2^{20} = 1048576$, and the state evolution has to be predicted for 20 steps into the future. In contrast to this, when using the move blocking scheme, the total number of sequences

is $2^{11} = 2048$, and the evolution of the state needs to be calculated only for 11 steps. As a result, the computations required are decreased by three orders of magnitude, or 99.9%.

It is important to point out that a high timing resolution is required only around the current time-step and the very near future. Further ahead, a rough timing resolution suffices, due to the receding horizon policy. The coarse plan of the second part of the prediction horizon is step by step shifted towards the beginning of the prediction horizon and simultaneously refined.

D. Load Uncertainty

In most applications the load is unknown and time varying. Thus, an external estimation loop should be added, which allows the elimination of the output voltage error in the presence of load uncertainties. This additional loop is employed to provide state estimates to the previously derived optimal controller, where the load was assumed to be known and constant. The output voltage reference will be adjusted so as to compensate for the deviation of the output voltage from its actual reference.

To achieve this, a discrete-time Kalman filter [36] is designed similar to [25]; thanks to its integrating nature the Kalman filter provides a zero steady-state output voltage error. Two integrating disturbance states, i_e and v_e, are introduced in order to model the effect of the load variations on the inductor current and output voltage, respectively. The measured state variables, i_L and v_o, together with the disturbance state variables form the augmented state vector

$$x_a = [i_L \; v_o \; i_e \; v_e]^T . \tag{9}$$

The Kalman filter is used to estimate the state vector given by (9). Depending on the operating mode of the converter, as shown in Fig. 3, four different affine systems result. The respective stochastic discrete-time state equations of the augmented model are

$$x_a(k+1) = E_{za} x_a(k) + F_{za} v_s(k) + \xi(k) , \tag{10}$$

where $z = \{1, 2, 3, 4\}$ corresponds to the four operating modes of the converter.

The measured state vector is given by

$$x(k) = \begin{bmatrix} i_L(k) \\ v_o(k) \end{bmatrix} = G_a x_a(k) + \nu(k) \tag{11}$$

and the matrices are

$$E_{za} = \begin{bmatrix} E_z & \mathbf{0} \\ \mathbf{0} & \mathbf{1} \end{bmatrix}, \; F_{1a} = \begin{bmatrix} F_1 \\ 0 \\ 0 \end{bmatrix} = F_{2a} = \begin{bmatrix} F_2 \\ 0 \\ 0 \end{bmatrix}, \; F_{3a} = \begin{bmatrix} F_3 \\ 0 \\ 0 \end{bmatrix},$$
$$F_{4a} = \begin{bmatrix} 0 & 0 & 0 & 0 \end{bmatrix}^T, \quad \text{and} \quad G_a = \begin{bmatrix} \mathbf{1} & \mathbf{1} \end{bmatrix}, \tag{12}$$

where, $\mathbf{1}$ is the identity matrix of dimension two and $\mathbf{0}$ are square zero matrices of dimension two. The variables $\xi \in \mathbb{R}^4$ and $\nu \in \mathbb{R}^2$ denote the process and the measurement noise, respectively. These terms represent zero-mean, white Gaussian noise sequences with normal probability distributions. Their covariances are given by $E[\xi\xi^T] = Q$ and $E[\nu\nu^T] = R$, and are positive semi-definite and positive definite, respectively.

A switched discrete-time Kalman filter is designed based on the augmented model of the converter. The active mode of the Kalman filter (one out of four) is determined by the switching position and the operating mode of the converter.

Due to the fact that the state-update for each operating mode is different, four Kalman gains K_z need to be calculated. Consequently, the equation for the estimated state $\hat{x}_a(k)$ is

$$\hat{x}_a(k+1) = E_{za}\hat{x}_a(k) + K_z G_a\big(x_a(k) - \hat{x}_a(k)\big) + F_{za} v_s(k) . \tag{13}$$

The noise covariance matrices Q and R are chosen such that high credibility is assigned to the measurements of the physical states (i_L and v_o), whilst low credibility is assigned to the dynamics of the disturbance states (i_e and v_e). The Kalman gains are calculated based on these matrices. The estimated disturbances, provided by the resulting filter, can be used to remove their influence from the output voltage. Hence, the disturbance state $\hat{v}_e$ is used to adjust the output voltage reference $v_{o,ref}$

$$\tilde{v}_{o,ref} = v_{o,ref} - \hat{v}_e . \tag{14}$$

To this end, the estimated states, $\hat{i}_L$ and $\hat{v}_o$, are used as inputs to the controller, instead of the measured states, i_L and v_o.

E. Control Algorithm

The proposed control concept is summarized in Algorithm 1. The function f stands for the state-update given by (4), with the subscripts 1 and 2 corresponding to the sampling interval being used, i.e. T_s and $n_s T_s$, respectively. Fig. 7 depicts the flowchart of the introduced MPC algorithm, while

Algorithm 1 MPC algorithm

function $u^*(k)$ = MPC ($\hat{x}(k), u(k-1)$)
  $J^*(k) = \infty$; $u^*(k) = \emptyset$; $x(k) = \hat{x}(k)$
  for all U over N **do**
    $J = 0$
    for $\ell = k$ to $k + N - 1$ **do**
      if $\ell < k + N_1$ **then**
        $x(\ell+1) = f_1(x(\ell), u(\ell))$
      else
        $x(\ell+1) = f_2(x(\ell), u(\ell))$
      end if
      $v_{o,err}(\ell+1) = \tilde{v}_{o,ref} - v_o(\ell+1)$
      $\Delta u(\ell) = u(\ell) - u(\ell-1)$
      $J = J + |v_{o,err}(\ell+1)| + \lambda|\Delta u(\ell)|$
    end for
    if $J < J^*(k)$ **then**
      $J^*(k) = J$, $u^*(k) = U(1)$
    end if
  end for
end function

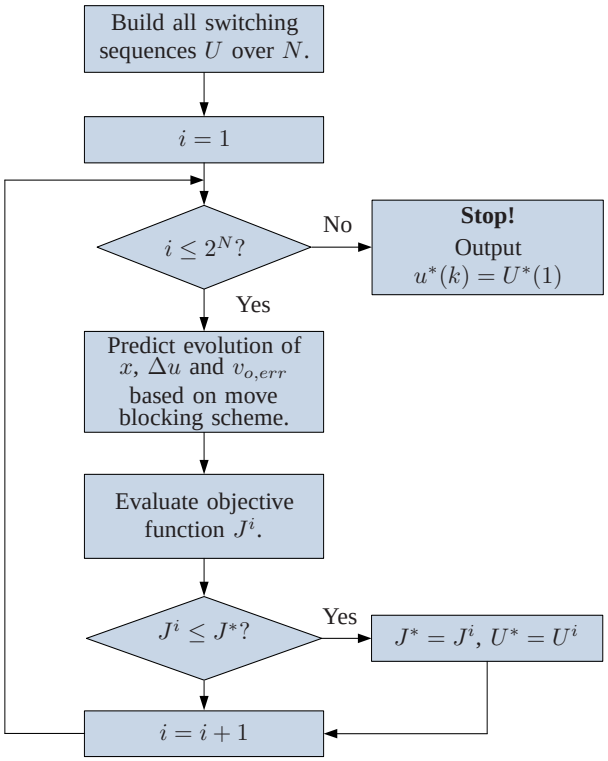

Fig. 7. Flowchart of the MPC algorithm.

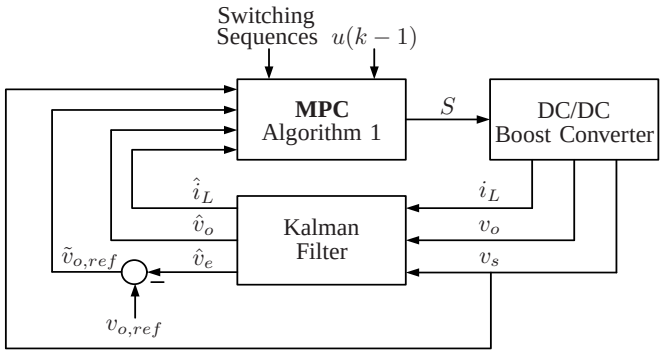

Fig. 8. Block diagram of the MPC scheme and Kalman filter.

the block diagram of the entire control scheme is shown in Fig. 8.

V. Simulation Results

In this section simulation results are presented to demonstrate the performance of the proposed controller under several operating conditions. Specifically, the closed-loop converter behavior is examined in both CCM and DCM. The dynamic performance is investigated during start-up. Moreover, the responses of the output voltage to step changes in the commanded voltage reference, the input voltage and the load are illustrated.

The circuit parameters are $L = 450\,\mu$H, $R_L = 0.3\,\Omega$ and $C_o = 220\,\mu$F. The nominal load resistance is $R = 73\,\Omega$. If not otherwise stated, the input voltage is $v_s = 10\,$V and the reference of the output voltage is $v_{o,ref} = 15\,$V.

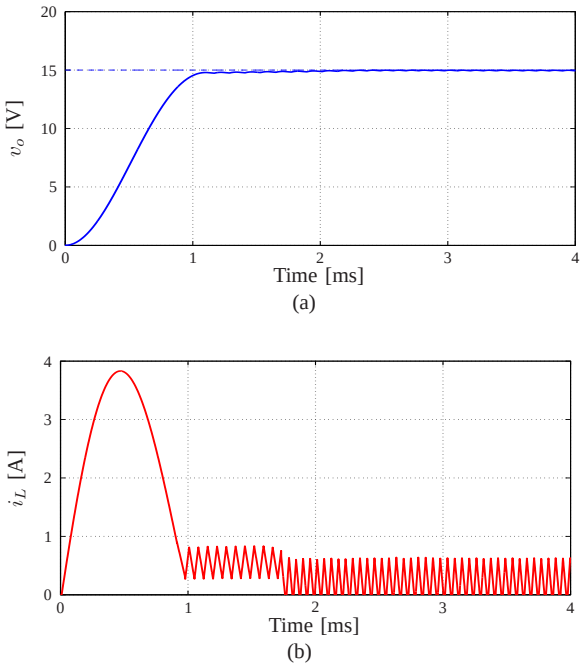

Fig. 9. Simulation results for nominal start-up: a) output voltage (solid line) and output voltage reference (dashed line), b) inductor current.

The weight in the objective function is $\lambda = 0.1$, the prediction horizon is $N = 14$ and the sampling interval is $T_s = 2.5\,\mu$s. A move blocking scheme is used with $N_1 = 8$, $N_2 = 6$ and $n_s = 4$, i.e. the sampling interval for each of the last six steps in the prediction interval is $T_s = 10\,\mu$s[2]. Finally, the covariance matrices of the Kalman filter are chosen as $Q = \mathrm{diag}(0.1, 0.1, 50, 50)$ and $R = \mathrm{diag}(1, 1)$.

A. Start-Up

The first case to be examined is that of the start-up behavior under nominal conditions. As can be seen in Fig. 9, the inductor current is very quickly increased until the capacitor is charged to the desired voltage level. The output voltage reaches its reference value in about $t \approx 1.8\,$ms, without any noticeable overshoot. Subsequently, the converter operates in DCM with the inductor current reaching zero.

B. Step Changes in the Output Reference Voltage

Next, step changes in the reference of the output voltage are considered. First, a step-up change in the output reference voltage is examined: at time $t = 2\,$ms the reference is doubled from $v_{o,ref} = 15\,$V to $v_{o,ref} = 30\,$V. As can be seen in Fig. 10, the controller increases the current temporarily in order to quickly ramp up the output voltage. Note that this favorable choice is made by the controller thanks to its long prediction horizon and *despite* the non-minimum phase

[2]The length of the prediction horizon in time should be as long as possible. A horizon of about 80 μs is sufficient. The first part of the prediction horizon should be finely sampled, since switching is possible only at the sampling instants. As such, the sampling interval T_s should be as small as possible. The number of steps in the prediction horizon $N = N_1 + N_2$ determines the computational complexity. To ensure that the control law can be computed within T_s, N should be relatively small, leading to the choice made above.

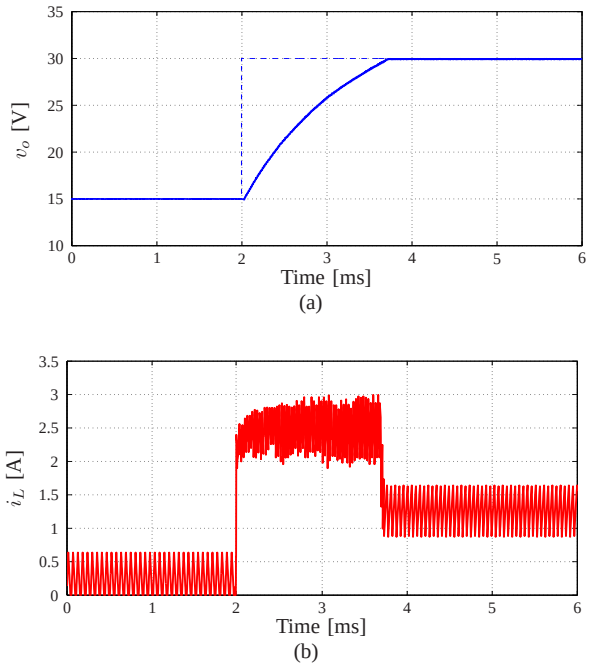

Fig. 10. Simulation results for a step-up change in the output voltage reference: a) output voltage (solid line) and output voltage reference (dashed line), b) inductor current.

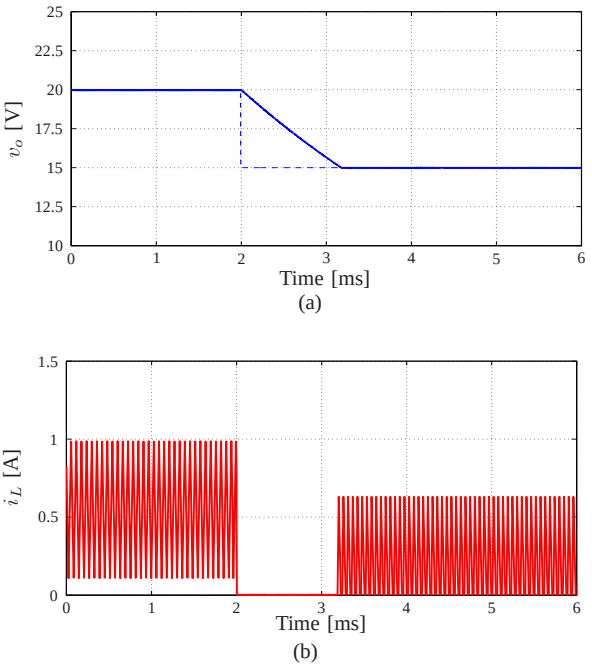

Fig. 11. Simulation results for a step-down change in the output voltage reference: a) output voltage (solid line) and output voltage reference (dashed line), b) inductor current.

behavior of the converter. Once the output voltage has reached its reference, the inductor current is decreased to the level that corresponds to the steady-state power balance. The controller exhibits an excellent behavior during the transient, reaching the new output voltage in about $t \approx 1.8\,\text{ms}$, without any overshoot.

Furthermore, the behavior of the controller is tested under a step-down change in the output reference voltage. At time $t = 2\,\text{ms}$, the output voltage reference changes from $v_{o,ref} = 20\,\text{V}$ to $v_{o,ref} = 15\,\text{V}$; the segment of interest is depicted in Fig. 11. Since the proposed MPC strategy is formulated as a voltage-mode controller effort is put into decreasing the voltage to its new desired level as quickly as possible. To do so, the controllable switch is turned off, the current instantaneously reaches zero, and the capacitor discharges through the load until it reaches its new demanded value in about $t \approx 1.2\,\text{ms}$.

C. Step Change in the Input Voltage

Operating at the steady-state operating point corresponding to $v_{o,ref} = 30\,\text{V}$, the input voltage is changed in a step-wise fashion. At time $t = 0.4\,\text{ms}$ the input voltage is increased from $v_s = 10\,\text{V}$ to $v_s = 15\,\text{V}$. The transient response of the converter is depicted in Fig. 12. The output voltage remains practically unaffected, with no undershoot observed, while the controller settles very quickly at the new steady-state operating point.

D. Load Step Change

The last case examined is that of a drop in the load resistance. As can be seen in Fig. 13, a step-down change

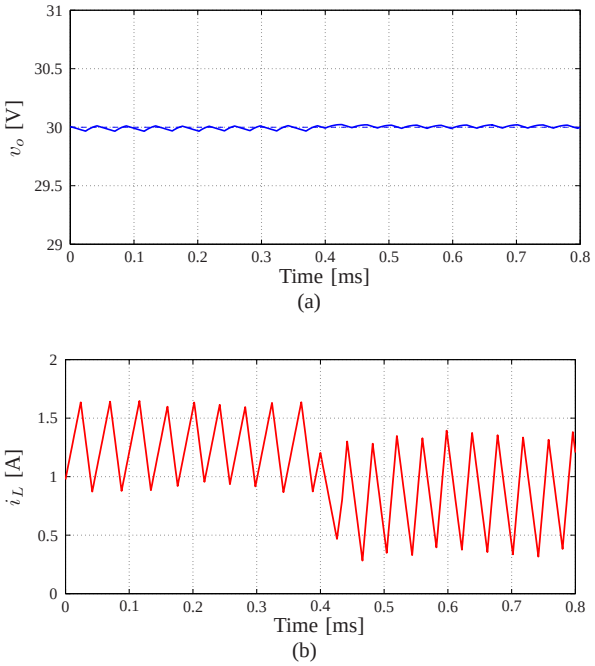

Fig. 12. Simulation results for a step-up change in the input voltage: a) output voltage (solid line) and output voltage reference (dashed line), b) inductor current.

in the load from $R = 73\,\Omega$ to $R = 36.5\,\Omega$ occurs at $t = 1\,\text{ms}$, while the input voltage is $v_s = 15\,\text{V}$, and the output voltage reference $v_{o,ref} = 30\,\text{V}$. The Kalman filter adjusts the output voltage reference to its new value so as to avoid any steady-state tracking error. This can be observed in Fig. 13(a); after the converter has settled at the new operating point, the output voltage accurately follows its reference.

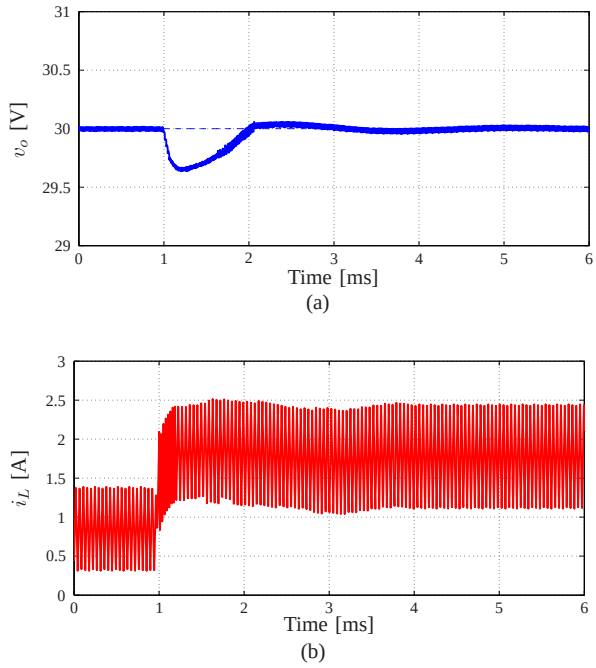

Fig. 13. Simulation results for a step-down change in the load: a) output voltage (solid line) and output voltage reference (dashed line), b) inductor current.

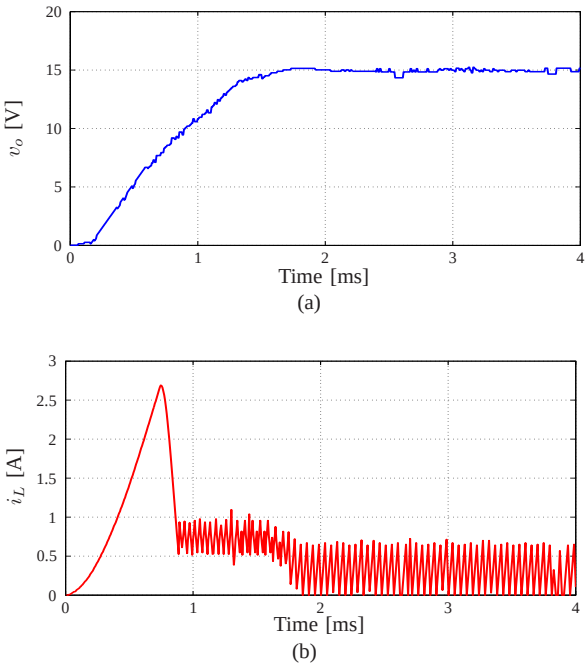

Fig. 14. Experimental results for nominal start-up: a) output voltage, and b) inductor current.

VI. Experimental Validation

To further investigate the potential advantages of the proposed algorithm, the controller was implemented on a dSpace DS1104 real-time system. A boost converter was built using an IRF60 MOSFET and a MUR840 diode as active and passive switches, respectively. The values of the circuit elements are the same as in Section V. Moreover, the nominal input and output voltages and the nominal load resistance are the same as previously. The voltage and current measurements were obtained using Hall effect transducers.

Due to computational restrictions imposed by the computational platform, a six-step prediction horizon was implemented, i.e. $N = 6$ and the sampling interval was set to $T_s = 10\,\mu$s. The prediction horizon was split into $N_1 = 4$ and $N_2 = 2$ with $n_s = 2$. The weight in the objective function was chosen as $\lambda = 0.5$. The covariance matrices of the Kalman filter are the same as previously.

A. Start-up

In Fig. 14 the output voltage and the inductor current of the converter are depicted during start-up. The inductor current rapidly increases to charge the output capacitor to the reference voltage level as fast as possible. The output voltage reaches its desired value in about $t \approx 1.8\,$ms. Subsequently, the inductor current reaches its nominal value and the converter operates in DCM.

B. Step Changes in the Output Reference Voltage

The second case to be analyzed is that of the transient behavior during step changes in the output reference voltage. A step-up change in the output reference voltage from $v_{o,ref} = 15\,\text{V}$ to $v_{o,ref} = 30\,\text{V}$ occurs at $t \approx 1.7\,$ms. The response of the converter is illustrated in Fig. 15. The inductor current instantaneously increases, enabling the output voltage to reach its new desired level as fast as possible. This happens in about $t \approx 1.9\,$ms, without a significant overshoot. Moreover, a step-down change, illustrated in Fig. 16, is investigated. The output reference voltage changes from $v_{o,ref} = 20\,\text{V}$ to $v_{o,ref} = 15\,\text{V}$ at $t \approx 1.9\,$ms. As can be seen, the controller

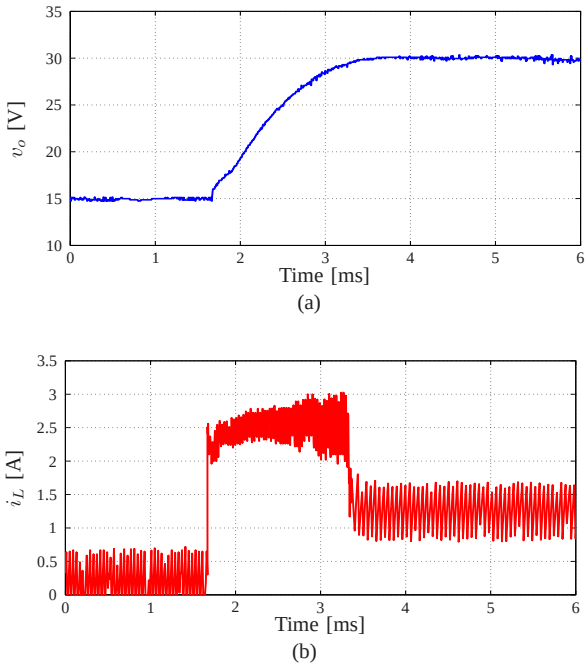

Fig. 15. Experimental results for a step-up change in the output voltage reference: a) output voltage, and b) inductor current.

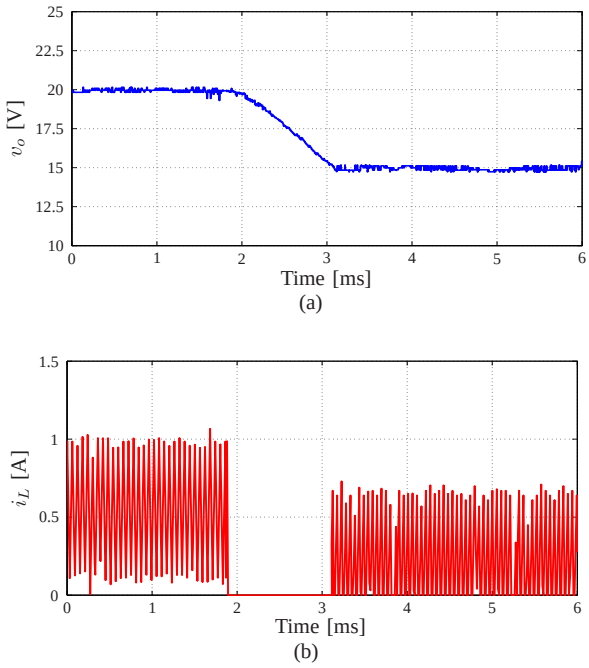

Fig. 16. Experimental results for a step-down change in the output voltage reference: a) output voltage, and b) inductor current.

exhibits a favorable performance; the inductor current is instantly reduced to zero so as to allow the capacitor to discharge through the resistor, and the converter reaches the new steady-state operating point in about $t \approx 1.2\,\text{ms}$.

C. Ramp Change in the Input Voltage

Subsequently, the input voltage is manually increased from $v_s = 10\,\text{V}$ to $v_s = 15\,\text{V}$ (the output reference voltage is $v_{o,ref} = 30\,\text{V}$), resulting in a voltage ramp from $t \approx 16\,\text{ms}$ until $t \approx 38\,\text{ms}$. During the transient, the inductor current changes accordingly in a ramp-like manner down to its new steady-state value. It can be seen that the output voltage remains unaffected and is kept equal to its reference value, implying that input voltage disturbances are very effectively rejected by the controller and the Kalman filter.

D. Load Step Change

The last case examined is that of a step-down change in the load resistance occurring at $t \approx 1.2\,\text{ms}$. With the converter operating at the previously attained operating point, the load resistance is halved, i.e. from $R = 73\,\Omega$ to $R = 36.5\,\Omega$. As can be observed in Fig. 18, the Kalman filter quickly adjusts the voltage reference accordingly, resulting in a zero steady-state error in the output voltage, thanks to its integrating nature.

VII. Conclusion

A model predictive control approach based on enumeration for dc-dc boost converter is proposed that directly regulates the output voltage along its reference, without the use of an underlying current control loop. This enables very fast dynamics during transients. Since the converter model is included in the controller, the time-consuming tuning of

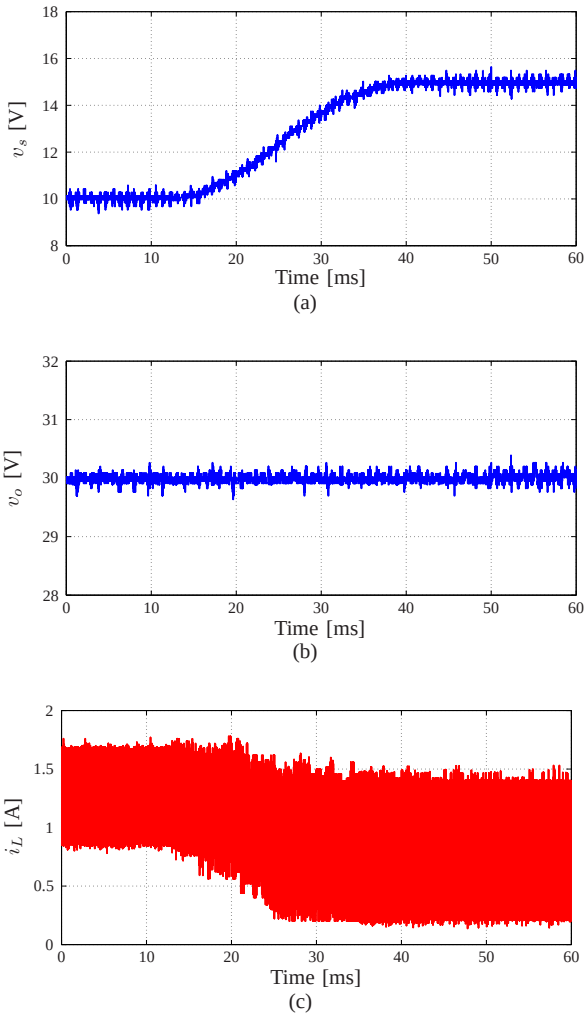

Fig. 17. Experimental results for a ramp change in the input voltage: a) input voltage, b) output voltage, and c) inductor current.

controller gains is avoided. The computational complexity is somewhat pronounced, but kept at bay by using a move blocking scheme. In addition to that, the switching frequency is variable. A load estimation scheme, namely a discrete-time switched Kalman filter, is implemented to address load variations and to ensure robustness to parameter variations. Simulation and experimental results demonstrate the potential advantages of the proposed methodology.

References

[1] N. Mohan, T. M. Undeland, and W. P. Robbins, *Power Electronics: Converters, Applications and Design*, 3rd ed. Hoboken, NJ: Wiley, 2003.

[2] R. W. Erickson, S. Ćuk, and R. D. Middlebrook, "Large-signal modelling and analysis of switching regulators," in *Proc. IEEE Power Electron. Spec. Conf.*, Cambridge, MA, Jun. 1982, pp. 240–250.

[3] J. Álvares-Ramírez, I. Cervantes, G. Espinosa-Pérez, P. Maya, and A. Morales, "A stable design of PI control for dc-dc converters with an RHS zero," *IEEE Trans. Circuits Syst. I*, vol. 48, no. 1, pp. 103–106, Jan. 2001.

[4] T. Gupta, R. R. Boudreaux, R. M. Nelms, and J. Y. Hung, "Implementation of a fuzzy controller for dc-dc converters using an inexpensive 8-b microcontroller," *IEEE Trans. Ind. Electron.*, vol. 44, no. 5, pp. 661–669, Oct. 1997.

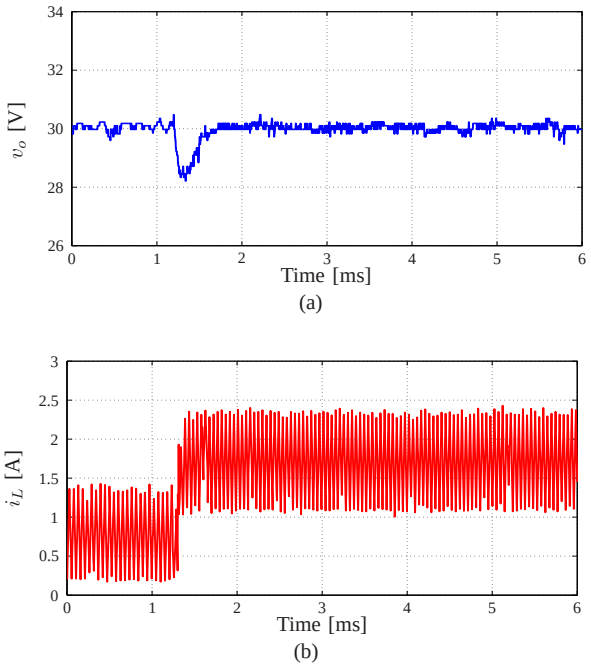

Fig. 18. Experimental results for a step-down change in the load: a) output voltage, and b) inductor current.

[5] P. Mattavelli, L. Rossetto, G. Spiazzi, and P. Tenti, "General-purpose fuzzy controller for dc-dc converters," *IEEE Trans. Power Electron.*, vol. 12, no. 1, pp. 79–86, Jan. 1997.

[6] H. J. Sira-Ramírez, "Nonlinear P-I controller design for switchmode dc-to-dc power converters," *IEEE Trans. Circuits Syst. I*, vol. 38, no. 4, pp. 410–417, Apr. 1991.

[7] S. Hiti and D. Borojević, "Robust nonlinear control for the boost converter," *IEEE Trans. Power Electron.*, vol. 10, no. 6, pp. 651–658, Nov. 1995.

[8] M. K. Kazimierczuk and A. Massarini, "Feedforward control dynamic of dc/dc PWM boost converter," *IEEE Trans. Circuits Syst. I*, vol. 44, no. 2, pp. 143–149, Feb. 1997.

[9] M. K. Kazimierczuk and L. A. Starman, "Dynamic performance of PWM dc/dc boost converter with input voltage feedforward control," *IEEE Trans. Circuits Syst. I*, vol. 46, no. 12, pp. 1473–1481, Dec. 1999.

[10] P. Mattavelli, L. Rossetto, and G. Spiazzi, "Small-signal analysis of dc-dc converters with sliding mode control," *IEEE Trans. Power Electron.*, vol. 12, no. 1, pp. 96–102, Jan. 1997.

[11] S.-C. Tan, Y. M. Lai, and C. K. Tse, "General design issues of sliding-mode controllers in dc-dc converters," *IEEE Trans. Ind. Electron.*, vol. 55, no. 3, pp. 1160–1174, Mar. 2008.

[12] A. Kugi and K. Schlacher, "Nonlinear H_∞ controller design for a dc-to-dc power converter," *IEEE Trans. Contr. Syst. Technol.*, vol. 7, no. 2, pp. 230–237, Mar. 1999.

[13] D. Q. Mayne, J. B. Rawlings, C. V. Rao, and P. O. M. Scokaert, "Constrained model predictive control: Stability and optimality," *Automatica*, vol. 36, no. 6, pp. 789–814, Jun. 2000.

[14] J. B. Rawlings and D. Q. Mayne, *Model Predictive Control: Theory and Design*. Madison, WI: Nob Hill, 2009.

[15] T. Geyer, "Low complexity model predictive control in power electronics and power systems," Ph.D. dissertation, Autom. Control Lab. ETH, Zurich, 2005.

[16] P. Correa, M. Pacas, and J. Rodríguez, "A predictive torque control for inverter-fed induction machines," *IEEE Trans. Ind. Electron.*, vol. 54, no. 2, pp. 1073–1079, Apr. 2007.

[17] T. Geyer, G. Papafotiou, and M. Morari, "Model predictive direct torque control—Part I: Concept, algorithm and analysis," *IEEE Trans. Ind. Electron.*, vol. 56, no. 6, pp. 1894–1905, Jun. 2009.

[18] P. Cortés, M. P. Kazmierkowski, R. M. Kennel, D. E. Quevedo, and J. Rodríguez, "Predictive control in power electronics and drives," *IEEE Trans. Ind. Electron.*, vol. 55, no. 12, pp. 4312–4324, Dec. 2008.

[19] P. Cortés, J. Rodríguez, P. Antoniewicz, and M. Kazmierkowski, "Direct power control of an AFE using predictive control," *IEEE Trans. Power Electron.*, vol. 23, no. 5, pp. 2516–2523, Sep. 2008.

[20] A. Nami, F. Zare, A. Ghosh, and F. Blaabjerg, "A hybrid cascade converter topology with series-connected symmetrical and asymmetrical diode-clamped H-bridge cells," *IEEE Trans. Power Electron.*, vol. 26, no. 1, pp. 51–65, Jan. 2011.

[21] S. Bibian and H. Jin, "High performance predictive dead-beat digital controller for dc power supplies," *IEEE Trans. Power Electron.*, vol. 17, no. 3, pp. 420–427, May 2002.

[22] J. Chen, A. Prodić, R. W. Erickson, and D. Maksimović, "Predictive digital current programmed control," *IEEE Trans. Power Electron.*, vol. 18, no. 1, pp. 411–419, Jan. 2003.

[23] F. M. Oettmeier, J. Neely, S. Pekarek, R. DeCarlo, and K. Uthaichana, "MPC of switching in a boost converter using a hybrid state model with a sliding mode observer," *IEEE Trans. Ind. Electron.*, vol. 56, no. 9, pp. 3453–3466, Sep. 2009.

[24] T. Geyer, G. Papafotiou, and M. Morari, "On the optimal control of switch-mode dc-dc converters," in *Hybrid Syst.: Comput. and Control*, ser. LNCS, R. Alur and G. J. Pappas, Eds. Berlin, Germany: Springer-Verlag, 2004, vol. 2993, pp. 342–356.

[25] T. Geyer, G. Papafotiou, R. Frasca, and M. Morari, "Constrained optimal control of the step-down dc-dc converter," *IEEE Trans. Power Electron.*, vol. 23, no. 5, pp. 2454–2464, Sep. 2008.

[26] A. G. Beccuti, G. Papafotiou, R. Frasca, and M. Morari, "Explicit hybrid model predictive control of the dc-dc boost converter," in *Proc. IEEE Power Electron. Spec. Conf.*, Orlando, FL, Jun. 2007, pp. 2503–2509.

[27] A. G. Beccuti, S. Mariéthoz, S. Cliquennois, S. Wang, and M. Morari, "Explicit model predictive control of dc-dc switched-mode power supplies with extended Kalman filtering," *IEEE Trans. Ind. Electron.*, vol. 56, no. 6, pp. 1864–1874, Jun. 2009.

[28] Y. Xie, R. Ghaemi, J. Sun, and J. S. Freudenberg, "Implicit model predictive control of a full bridge dc-dc converter," *IEEE Trans. Power Electron.*, vol. 24, no. 12, pp. 2704–2713, Dec. 2009.

[29] P. Karamanakos, G. Papafotiou, and S. Manias, "Model predictive control strategies for dc-dc boost voltage conversion," in *Proc. Eur. Power Electron. Conf.*, Birmingham, UK, Aug./Sep. 2011, pp. 1–9.

[30] P. Karamanakos, T. Geyer, and S. Manias, "Direct model predictive current control of dc-dc boost converters," in *Proc. Int. Power Electron. and Motion Control Conf. and Expo.*, Novi Sad, Serbia, Sep. 2012, pp. DS2c.11–1–DS2c.11–8.

[31] T. Geyer, G. Papafotiou, and M. Morari, "Hybrid model predictive control of the step-down dc-dc converter," *IEEE Trans. Contr. Syst. Technol.*, vol. 16, no. 6, pp. 1112–1124, Nov. 2008.

[32] R. Cagienard, P. Grieder, E. C. Kerrigan, and M. Morari, "Move blocking strategies in receding horizon control," *J. of Process Control*, vol. 17, no. 6, pp. 563–570, Jul. 2007.

[33] R. W. Erickson and D. Maksimović, *Fundamentals of Power Electronics*, 2nd ed. Norwell, MA: Kluwer Academic, 2001.

[34] A. Bemporad and M. Morari, "Control of systems integrating logic, dynamics and constraints," *Automatica*, vol. 35, no. 3, pp. 407–427, Mar. 1999.

[35] T. Geyer, G. Papafotiou, and M. Morari, "Model predictive control in power electronics: A hybrid systems approach," in *Proc. IEEE Conf. Decis. Control*, Seville, Spain, Dec. 2005, pp. 5606–5611.

[36] G. Pannocchia and J. B. Rawlings, "Disturbance models for offset-free model-predictive control," *AIChE J.*, vol. 49, no. 2, pp. 426–437, Feb. 2003.